
STOCHASTIC GRADIENT LANGEVIN WITH DELAYED GRADIENTS

Vyacheslav Kungurtsev*
 Department of Computer Science
 Czech Technical University in Prague
 kunguvya@fel.cvut.cz

Bapi Chatterjee†
 Institute of Science and Technology
 Austria
 bapi.chatterjee@ist.ac.at

Dan Alistarh‡
 Institute of Science and Technology
 Austria
 dan.alistarh@ist.ac.at

ABSTRACT

Stochastic Gradient Langevin Dynamics (SGLD) ensures strong guarantees with regards to convergence in measure for sampling log-concave posterior distributions by adding noise to stochastic gradient iterates. Given the size of many practical problems, parallelizing across several asynchronously running processors is a popular strategy for reducing the end-to-end computation time of stochastic optimization algorithms. In this paper, we are the first to investigate the effect of asynchronous computation, in particular evaluation of stochastic Langevin gradients at delayed iterates, on the convergence in measure. For this, we exploit recent results modeling Langevin dynamics as solving a convex optimization problem on the space of measures. We show that the rate of convergence in measure is not significantly affected by the error caused by the delayed gradient information used for computation, suggesting significant potential for speedup in wall clock time. We confirm our theoretical results with numerical experiments on some practical problems.

1 Introduction

In this paper we are interested in performing stochastic gradient Langevin dynamics (SGLD) for Bayesian learning. SGLD is a subsampling-based MCMC algorithm based on combining ideas from stochastic optimization, in particular the stochastic gradient method [11] with Langevin dynamics, a framework using the Langevin stochastic differential equation to model a gradient based Markov Chain Monte Carlo (MCMC) method, first introduced in [12]. The aim of the procedure is to find the stationary distribution characterizing a potential,

$$\mu(x) = e^{-U(x)} / \int_{\mathbb{R}^d} e^{-U(x)} dx \quad (1)$$

with an algorithm that is in effect a discretization of the stochastic differential equation,

$$dX_t = -\nabla U(X_t)dt + \sqrt{2\sigma}B_t \quad (2)$$

where B_t is a Weiner Brownian motion noise, most typically the Euler-Marayama discretization

$$X_{k+1} = X_k - \gamma_k \nabla U(X_k) + \sqrt{2\sigma\gamma_k}G_k \quad (3)$$

*Support for this author was provided by the OP VVV project CZ.02.1.01/0.0/0.0/16_019/0000765 “Research Center for Informatics”

†Supported by the European Union’s Horizon 2020 research and innovation programme under the Marie Sklodowska-Curie grant agreement No. 754411 (ISTPlus).

‡This project has received funding from the European Research Council (ERC) under the European Union’s Horizon 2020 research and innovation programme (grant agreement No 805223).

where now G_{k+1} is a Gaussian random normal variable.

In this paper we are interested in analyzing the impact of using parallel hardware architecture to compute the gradients in an asynchronous manner so as to maximize the use of computational resources, thus resulting in stale gradient information in the computation of $\nabla U(\cdot)$, i.e., the formal algorithm describing the method becomes,

$$X_{k+1} = X_k - \gamma_k \nabla U(\hat{X}_k) + \sqrt{2\sigma\gamma_k} G_k \quad (4)$$

where $\hat{X}_k = X_{k-\tau_k}$ with $\tau_k \leq \tau$ for some maximum delay τ , which corresponds to the consistent read/write environment. The theoretical analysis of such a method is not straightforward, as stochastic differential equations with delays presents a number of challenges. However, we found that the analysis in [4], analyzing Langevin dynamics from the perspective of convex optimization in the Wasserstein space of order two to be conveniently suitable.

In the literature we have found two works on implementing Langevin dynamics with distributed computing. The paper [1] considers (3) with a constant stepsize and analyzes the asymptotic solution properties, in particular the bias and the variance of the limit point. In [8] the downpour and elastic distributed computing frameworks were studied in the theoretical and numerical convergence properties of their iterates. They also analyzed the bias and variance estimation properties of the iterates generated by these methods.

By contrast, in this paper we are interested in performing a standard canonical convergence analysis of Langevin dynamics with stale gradients, in particular focusing on the convergence rate in the distance to the optimal posterior stationary distribution in the metrics of information theory, namely the KL divergence and Wasserstein distance. This is a standard type of result sought after for this class of problems, appearing in classic and well-cited references such as [10] and [2], for instance. In addition, we validate our analysis with numerical experiments, considering classical problems for posterior Bayesian estimation and showcasing the convergence and speedup properties of parallelization.

We shall consider the vectors of interest as living in the space \mathbb{R}^d . We now introduce some notation following [4]. A transference plan $\zeta(\mu, \nu)$ of two probability measures μ and ν is itself a probability measure on $(\mathbb{R}^d \times \mathbb{R}^d, \mathcal{B}(\mathbb{R}^d \times \mathbb{R}^d))$ such that for all measurable $A \subseteq \mathbb{R}^d$, it holds that $\zeta(A \times \mathbb{R}^d) = \mu(A)$ and $\zeta(\mathbb{R}^d \times A) = \nu(A)$. We denote by $\Pi(\mu, \nu)$ the set of transference plans of μ and ν . A couple of \mathbb{R}^d valued random variables (X, Y) is a coupling of μ and ν if there exists a $\zeta \in \Pi(\mu, \nu)$ such that (X, Y) are distributed according to ζ . The Wasserstein distance of order two is,

$$W_2(\mu, \nu) = \left(\inf_{\zeta \in \Pi(\mu, \nu)} \int_{\mathbb{R}^d \times \mathbb{R}^d} \|x - y\|^2 d\zeta(x, y) \right)^{1/2}.$$

For all μ, ν there exists a $\zeta^* \in \Pi(\mu, \nu)$ realizing the *inf*, i.e., for any coupling (X, Y) distributed according to ζ^* we have $W_2(\mu, \nu) = \mathbb{E}[\|X - Y\|^2]^{1/2}$, called the optimal transference plan and optimal coupling associated with W_2 . The space $\mathcal{P}_2(\mathbb{R}^d)$ is the set of finite second moment probability measures and together with W_2 is a complete separable metric space.

Now if $\mu \ll \nu$, i.e., μ is absolutely continuous w.r.t. ν , we define the Kullback-Leibler (KL) divergence of μ from ν by,

$$KL(\mu|\nu) = \begin{cases} \int_{\mathbb{R}^d} \frac{d\mu}{d\nu}(x) \log \left(\frac{d\mu}{d\nu}(x) \right), & \text{if } \mu \ll \nu, \\ \infty & \text{otherwise.} \end{cases}$$

We shall make the following assumptions,

Assumption 1.1. 1. $U : \mathbb{R}^d \rightarrow \mathbb{R}$ is strongly convex with convexity constant m , i.e., for all $x, y \in \mathbb{R}^d$ and $t \in [0, 1]$,

$$U(tx + (1-t)y) \leq tU(x) + (1-t)U(y) - t(1-t)(m/2)\|x - y\|^2$$

and

2. U is continuously Lipschitz differentiable, in particular with constant L , i.e.,

$$\|\nabla U(x) - \nabla U(y)\| \leq L\|x - y\|.$$

2 Convergence

We shall follow the structure of the convergence proof given in [4] and use a similar notation, modifying the components as necessary to account for asynchrony. First we note that we must define the continuous time variable \hat{X}_t , since the vector \hat{X}_k is only defined to correspond to a particular delay associated with the update at iteration k , and this delay can generally vary iteration to iteration. We need that \hat{X}_t is a random process whose distribution satisfies a condition relative to distributions of $\{X_s\}_{s \in [t-\tau, t]}$. In particular, we make the following assumption on \hat{X}_t ,

Assumption 2.1. The delayed iterate vector \hat{X}_t has a distribution $\hat{\mu}_t \in \mathcal{P}_2(\mathbb{R}^d)$ depending on $\{\mu_s\}_{s \in [t-\tau, t]}$, where μ_t is the distribution of X_t , such that $\hat{X}_t = X_s$ for some $s \in [t - \tau, t]$ for a.e. $\hat{\mu}_t$.

The free energy functional $\mathcal{F} = \mathcal{H} + \mathcal{E}$ is composed of the H-functional,

$$\mathcal{H}(\mu) = \begin{cases} \int_{\mathbb{R}^d} \frac{d\mu}{d\text{Leb}}(x) \log \left(\frac{d\mu}{d\text{Leb}}(x) \right) dx & \text{if } \mu \ll \text{Leb} \\ +\infty & \text{otherwise} \end{cases}$$

and the free energy,

$$\mathcal{E} = \int_{\mathbb{R}^d} U(x) d\mu(x).$$

Define now, for $\mathbf{A} \in \mathcal{B}(\mathbb{R}^d)$

$$\begin{aligned} S_\gamma(x, \mathbf{A}) &= \delta_{x-\gamma\nabla U(x)}(\mathbf{A}) \\ \hat{S}_\gamma(x, \hat{x}, \mathbf{A}) &= \delta_{x-\gamma\nabla U(\hat{x})}(\mathbf{A}) \end{aligned}$$

as well as,

$$\begin{aligned} R_\gamma(x, \mathbf{A}) &= (4\pi\gamma)^{-d/2} \int_{\mathbf{A}} \exp(-\|y - x - \gamma\nabla U(x)\|^2 / (4\gamma\sigma)) dy \\ \hat{R}_\gamma(x, \hat{x}, \mathbf{A}) &= (4\pi\gamma)^{-d/2} \int_{\mathbf{A}} \exp(-\|y - x - \gamma\nabla U(\hat{x})\|^2 / (4\gamma\sigma)) dy \end{aligned}$$

and

$$T_\gamma(x, \mathbf{A}) = (4\pi\gamma)^{-d/2} \int_{\mathbf{A}} \exp(-\|y - x\|^2 / (4\gamma\sigma)) dy.$$

The proof of the following result does not change.

Lemma 2.1 (Lemma 3 in [4]). Assume 1.1. For all $\mu \in \mathcal{P}_2(\mathbb{R}^d)$ and $\gamma > 0$,

$$\mathcal{E}(\mu T_\gamma) - \mathcal{E}(\mu) \leq Ld\gamma.$$

The next Lemma, similar to Lemma 4 in [4] has a modification to account for the error in the stale gradients. The proof of the Lemma is available in Appendix A.

Lemma 2.2. Assume 1.1. For all $\gamma \in (0, L^{-1})$ and $\mu, \hat{\mu}, \nu \in \mathcal{P}_2(\mathbb{R}^d)$ it holds that, for almost every $\hat{\mu}$,

$$\begin{aligned} 2\gamma\{\mathcal{E}(\mu\hat{S}_\gamma) - \mathcal{E}(\nu)\} &\leq (1 - m\gamma)W_2^2(\mu, \nu) - (1 - \gamma)W_2^2(\mu\hat{S}_\gamma, \nu) + \gamma^3(L + L^2) \int_{\mathbb{R}^d} \|\nabla U(x)\|^2 d\mu(x) \\ &\quad + \gamma \left(\frac{L^2}{2} + 2\gamma L^2 + \gamma^2(L^2 + L^4) \right) \int_{\mathbb{R}^d} \|x - \hat{x}\|^2 d\mu(x) \end{aligned}$$

The next result is unaffected by the delays.

Lemma 2.3 (Lemma 5 in [4]). For $\mu, \nu \in \mathcal{P}_2(\mathbb{R}^d)$, $\mathcal{H}(\nu) < \infty$. For all $\gamma > 0$,

$$2\gamma\{\mathcal{H}(\mu T_\gamma) - \mathcal{H}(\nu)\} \leq W_2^2(\mu, \nu) - W_2^2(\mu T_\gamma, \nu).$$

The next proposition is as in Proposition 2 in [4], which combines the previous three lemmas, and thus with the modification according to Lemma 2.2

Proposition 2.1. Assume 1.1. For all $\gamma \in (0, L^{-1})$ and $\mu, \hat{\mu} \in \mathcal{P}_2(\mathbb{R}^d)$, we have, for a.e. $\hat{\mu}$

$$\begin{aligned} 2\gamma\{\mathcal{F}(\mu\hat{R}_\gamma) - \mathcal{F}(\pi)\} &\leq (1 - m\gamma)W_2^2(\mu, \pi) - W_2^2(\mu\hat{R}_\gamma, \pi) + \gamma W_2^2(\mu\hat{S}_\gamma, \pi) + 2\gamma^2 Ld \\ &\quad + \gamma^3(L + L^2) \int_{\mathbb{R}^d} \|\nabla U(x)\|^2 d\mu(x) + \gamma \left(\frac{L^2}{4} + 2\gamma L^2 + \gamma^2(L^2 + L^4) \right) \int_{\mathbb{R}^d} \|x - \hat{x}\|^2 d\mu(x) \end{aligned}$$

Proof. This comes from the definition of \mathcal{F}

$$\mathcal{F}(\mu\hat{R}_\gamma) - \mathcal{F}(\pi) = \mathcal{E}(\mu\hat{R}_\gamma) - \mathcal{E}(\mu\hat{S}_\gamma) + \mathcal{E}(\mu\hat{S}_\gamma) - \mathcal{E}(\pi) + \mathcal{H}(\mu\hat{R}_\gamma) - \mathcal{H}(\pi)$$

and applying Lemmas 2.1, 2.2 and 2.3.

□

Now define two non-increasing sequences $(\gamma_k)_{k \in \mathbb{N}}$ and $\{\lambda_k\}_{k \in \mathbb{N}}$ and $\Gamma_{N, N+n} = \sum_{k=N+1}^{N+n} \gamma_k$, $\Lambda_{N, N+n} = \sum_{k=N+1}^{N+n} \lambda_k$. Let $\mu_0 \in \mathcal{P}_2(\mathbb{R}^d)$ be an initial distribution. The sequence of probability measures $(\nu_n^N)_{n \in \mathbb{N}}$ is defined for all $n, N \in \mathbb{N}, n \geq 1$ by,

$$\nu_n^N = \Lambda_{N, N+n}^{-1} \sum_{k=N+1}^{N+n} \lambda_k \mu_0 \hat{Q}_\gamma^k, \quad \hat{Q}_\gamma^k = \hat{R}_{\gamma_1} \cdots \hat{R}_{\gamma_k}$$

The following modification of Theorem 6 in [4] follows directly from Proposition 2.1. The proof is available in Appendix A.

Theorem 2.1. *Given Assumption 1.1 and 2.1, let γ_k and λ_k are two non-increasing sequences of positive real numbers with $\gamma_1 < \frac{1}{2(L^2+L^4)}$ and $\lambda_{k+1}(1 - m\gamma_{k+1})/\gamma_{k+1} \leq \lambda_k/\gamma_k$ and $\mu_0 \in \mathcal{P}_2(\mathbb{R}^d)$ and $N \in \mathbb{N}$. Then for all $n \in \mathbb{N}$, it holds that, for almost every realization of \hat{X} ,*

$$\begin{aligned} & KL(\nu_n^N | \pi) + \lambda_{N+n} W_2^2(\mu_0 Q_\gamma^{N+n}, \pi) / (2\gamma_{N+n} \Lambda_{N, N+n}) \\ & \leq \lambda_{N+1} (1 - m\gamma_{N+1}) W_2^2(\mu_0 Q_\gamma^N, \pi) / (2\gamma_{N+1} \Lambda_{N, N+n}) + \Lambda_{N, N+n}^{-1} \sum_{k=N+1}^{N+n} \gamma_k \lambda_k Ld \\ & \quad + \Lambda_{N, N+n}^{-1} \sum_{k=N+1-\tau}^{N+n} 2\gamma_k \lambda_k \tau^2 \sigma \left(\frac{L^2}{4} + 2\gamma_k L^2 + \gamma_k^2 (L^2 + L^4) \right) + (\Lambda_{N, N+n})^{-1} \sum_{k=N+1}^{N+n} W_2^2(\mu_0 \hat{S}_\gamma^k, \pi) \\ & \quad + (\Lambda_{N, N+n})^{-1} \sum_{k=N+1-\tau}^{N+n-1} \gamma_k^2 \left[\frac{L}{2} + \frac{L^2}{2} + \tau^2 \left(\frac{L^2}{4} + 2\gamma_k L^2 + \gamma_k^2 (L^2 + L^4) \right) \right] \mathbb{E}_{d\mu_k} \|\nabla U(X_k)\|^2 \end{aligned}$$

We now must assume a bound on the gradient norm.

Assumption 2.2. *Assume that,*

$$\mathbb{E}_{d\mu_t} \|\nabla U(x_t)\| \leq G$$

for all t .

From this we get the iteration complexity bound akin to Corollary 7 and 9 in [4].

Corollary 2.1. *Given Assumption 1.1, 2.1 and 2.2 and $\epsilon > 0$ and $\mu_0 \in \mathcal{P}_2(\mathbb{R}^d)$, if*

$$\begin{aligned} \gamma_\epsilon & \leq \min\{\gamma^1, \gamma^2, \gamma^3, \gamma^4, \gamma^5, \gamma^6\}/4, \\ \gamma^1 & = \epsilon (Ld + L^2 \tau^2 \sigma)^{-1} & \gamma^2 & = \epsilon^{1/2} ([L + L^2 + \tau^2 L^2] G^2)^{-1}, \\ \gamma^3 & = \epsilon^{1/2} \frac{m}{L\tau G} & \gamma^4 & = \epsilon^{2/3} \left(\frac{2\sigma}{1.65L + \sqrt{\sigma}\sqrt{m}} + 1.65(L/m) + \frac{\tau L \sqrt{\sigma}}{m} \right)^{-1} \\ \gamma^5 & = L^2 (L^2 + L^4)^{-1}, & \gamma^6 & = \frac{1}{12} \end{aligned}$$

and,

$$n_\epsilon \geq 2 \max\{\lceil W_2^2(\mu_0, \pi) \gamma_\epsilon^{-1} \epsilon^{-1} \rceil, \tau\}$$

it holds that $KL(\nu_{n_\epsilon} | \pi) \leq \epsilon$ for a.e. $d\hat{\mu}(\hat{x})$, where $\nu_{n_\epsilon} = n_\epsilon^{-1} \sum_{k=1}^{n_\epsilon} \mu_0 \hat{R}_{\gamma_\epsilon}^k$.

Likewise if,

$$\gamma_\epsilon \leq m \min\{\gamma^1, \gamma^2, \gamma^3, \gamma^4, \gamma^5, \gamma^6\}/8$$

then for $n_\epsilon \geq 2 \max\{\lceil \log(4W_2^2(\mu_0, \pi)/\epsilon) \gamma_\epsilon^{-1} m^{-1} \rceil, \log \tau\}$ we have that,

$$W_2^2(\mu_0 \hat{R}_{\gamma_\epsilon}^{n_\epsilon}, \pi) \leq \epsilon$$

Comparing these Corollary 2.1 to [4], it is clear that the presence of delays does not affect the order of the convergence, however, it contributes to the scaling of the stepsize and number of required iterations relative to the size of the maximum delay τ . Note that the bound on the gradient that is introduced, which is a new assumption required by the analysis, only affects a term involving ϵ^{-1} and thus is less likely to hurt the convergence for tighter tolerance requirements.

Inconsistent Read

Consider now the inconsistent read/write scenario, wherein one processor can be in the middle of reading the vector x in memory while another processor begins to write an update to the memory. In this case, it is not just that the entire vector that the gradients are being computed at is delayed, but any given component of the vector used in the computation of the gradient could be delayed by a different quantity of iterations.

The Assumption 2.1 changes to

Assumption 2.3. The delayed iterate vector \hat{X}_t has a distribution $\hat{\mu}_t \in \mathcal{P}_2(\mathbb{R}^d)$ depending on $\{\mu_s\}_{s \in [t-\tau, t]}$, where μ_t is the distribution of X_t , such that $[\hat{X}_t]_i = [X_{s_i}]_i$ for some $s_i \in [t-\tau, t]$ for all i for a.e. $\hat{\mu}_t$. Furthermore assume that there exists a $G > 0$ such that $\|\nabla U(x)\| \leq G$ for all x .

where we must add a uniform bound on the potential gradient as well. Now in the derivation of Theorem 2.1 we have that now,

$$\mathbb{E} [\|x_k - \hat{x}_k\|^2] \leq \sum_{l=k-\tau}^k \gamma_l \tau \mathbb{E} \left[\left\| \gamma_l^{1/2} \nabla U(\hat{x}_k) + \sqrt{2} G_{k+1} \right\|^2 \right]$$

and this right hand side cannot be bounded by any particular gradient evaluation. It is clear then that we are able to obtain the same results as in Corollary 2.1.

3 Numerical Results

3.1 Experiment Setting

Implementation platform. For variation, we use two different shared-memory settings:

M1: The first setup is a multi-socket multi-core non-uniform-memory-access (NUMA) workstation based shared-memory system. The workstation packs four Intel(R) Xeon(R) Gold 6150 CPUs running at 2.7 GHz totaling 72 cores (144 logical cores with hyperthreading). It runs on Ubuntu 18.04 Linux. In this system, we perform multiprocessing with $P \in \{18, 36, 72\}$ processes running concurrently. Due to NUMA, gradient updates over the shared-memory have clear asynchrony and are thereby delayed.

M2: The second setup is a GPU based shared-memory system. The graphics processor Nvidia GeForce RTX 2080 Ti has 4352 CUDA cores. It allows concurrent launch of CUDA kernels by multiple processes using Nvidia’s multi-process service (MPS). MPS utilizes Hyper-Q capabilities of the Turing architecture based GPU. It allocates parallel compute resources – the streaming multiprocessors (SMs) – to concurrent CPU-GPU connections based on their availability. Such resource allocation results in asynchrony and thereby delayed gradient updates. It runs on Ubuntu 18.04 Linux. In this setting, we use $P \in \{2, 4, 8\}$ processes running concurrently on the same GPU.

In both settings, we allow concurrent processes to use all the compute cores simultaneously by launching parallel threads. The load-balancing with respect to thread-level-parallelism (TLP) is offered and managed by the operating system and/or CUDA runtime. Effectively, roughly identical amount of parallelization is obtained even by asynchronous concurrency due to TLP over the shared-memory system. This system-constraint plays an important role in determining the behavior of asynchronous methods which we will describe in the experimental observations below. We use the open source Pytorch [9] library to implement the experiments.

We seed each of the experimental runs, still the asynchronous methods face system-dependent randomization with regards to updates at each iteration. Therefore, we take the average of three runs in the results.

Methods. We allow asynchrony in the update scheme in the following two variants:

W-Con The concurrent processes read the model X using locks. Effectively, in an asynchronous setting, the gradients are delayed yet the model read is consistent.

W-Icon In a different approach we allow both read and update of X to be lock-free and thereby inconsistent.

By contrast, a synchronous update scheme ensures that the read as well as the update of the shared model are consistent:

Sync To impose synchrony we use barriers before the gradient computation and the model is updated by the sum of the gradients computed by the processes. After synchronizing at a barrier, the participating processes read the current model vector in memory, followed by computing the stochastic gradient and adding noise to it, and then pass the noisy gradients to one of the processes, which we call *updater*. The updater sums the gradients and then updates X with the sum thereof. At this point, the processes again synchronize at the barrier before they read the model to compute the gradient.

Notice that, in **W-Con** the read lock ensures that a process cannot read a vector while simultaneously it is being updated, i.e., it is not possible for it to compute a gradient at some X whose components are partially updated from $X_{s-\tau_1}$ and others from $X_{s-\tau_2}$, $\tau_1 \neq \tau_2$. However, the gradients can be computed from delayed iterates, i.e., because other processors have updated the vector in the meantime, the gradient computation used for an update is stale. On the other hand, synchronous parallel computation not only avoids inconsistency due to asynchrony but also has the advantage of effectively reduced variance in stochastic gradients due to, practically, a larger batch update.

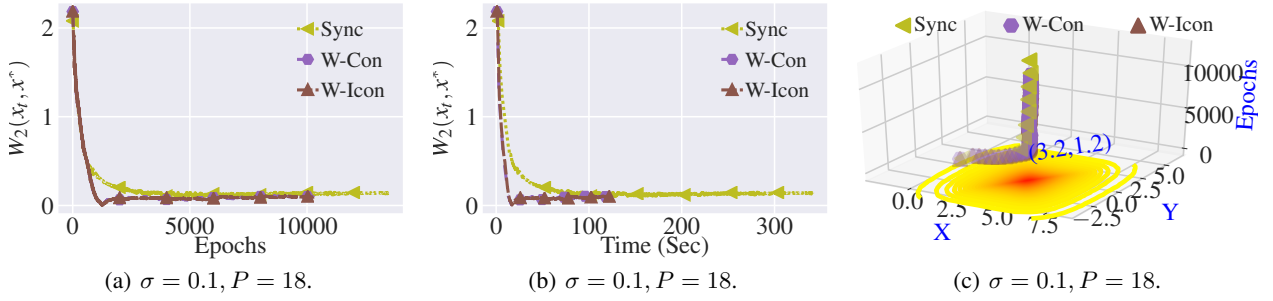


Figure 1: Optimization trajectory of the SGLD iterates are shown for training with 18 processes. Sub-figure (a) shows the convergence with respect to iterations (epochs), whereas, sub-figure (b) presents relative speed-up of the methods. In sub-figure (c), we depict the trajectory of iterates by tracking their first two co-ordinates. Sub-figure (c) also presents the contour plot of the potential $\exp(-U(x))$ near x^* on the plane $Epoch = 0$.

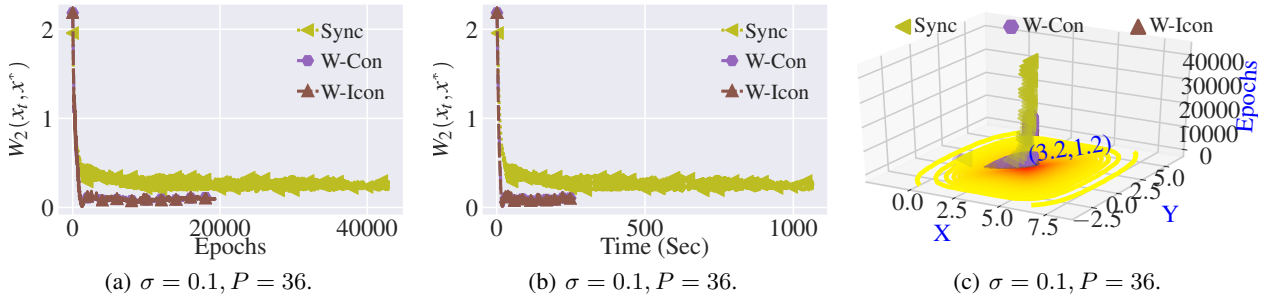


Figure 2: Optimization trajectory for training with 36 processes. Other descriptions are as those of Figure 1.

3.2 Regression

For the first test case we applied our asynchronous and synchronous variants of SGLD on a regression model. The implementation uses the CPU-based shared-memory setting **M1**. By implementation, our model is a single linear layer with 4 input features and an output feature implementing a 4th degree polynomial regression. First we randomly determine the actual polynomial coefficients we wish to fit with the regression. Then we run a sequential fully consistent stochastic gradient descent (SGD) scheme to obtain the mode of the posterior distribution x^* . Having obtained x^* , we seek to minimize the Wasserstein distance of order two of the SGLD iterates x_t from the posterior as defined by x^* , the potential and the noise, denoted as $W_2(x_t, x^*)$. We use the library [5] for $W_2(x_t, x^*)$ computation.

In the first set of experiments, we take $\nu_i \sim N(0, 0.1)$. We run the iterative scheme for 50,000 iterations and let it stop if the minimization of $W_2(x_t, x^*)$ plateaus for 500 consecutive iterations. We use an identical constant learning rate of 0.01, use a batch of 100,000 data samples to compute the initial stochastic gradient (note that the data set is essentially infinite as we can compute the output of the original actual polynomial to regress upon), and then add the additional $N(0, 0.1)$ noise at each iteration. The convergence behavior of SGLD iterates are presented in Figures 1, 2, and 3.

It is evident from the experimental observations that both the variants of asynchronous methods outperform the synchronous scheme with respect to both convergence, as seen in Figures 1(a), 2(a), 3(a) and speedup, see Figures 1(b), 2(b), 3(b). It is interesting to observe that both **W-Con** and **W-Icon** display better convergence in comparison to **Sync** updates despite of the fact that **Sync** faces reduced variance of stochastic gradients. Notice that as we increase the number of processes from 18 to 72, thereby increasing the batch-size for **Sync**, asynchronous methods perform even better. This observation corroborates the reduced competitiveness of large batch training without reducing the learning rate as noticed in [13]. In experiments we observed that on reducing the learning rate optimization of **Sync** improves by way of running for a much larger number of iterations, however, that also reveals the comparative efficacy of the small batch asynchronous methods.

To explore the effect of noise, we performed another set of experiments with $\nu_i \sim N(0, 1)$. The hyperparameters – learning rate, batch-size, etc. – are identical to those used before. The numerical results for training with 72 processes are presented in Figure 4; and results for other asynchrony cases are available in Appendix B. We observe that the

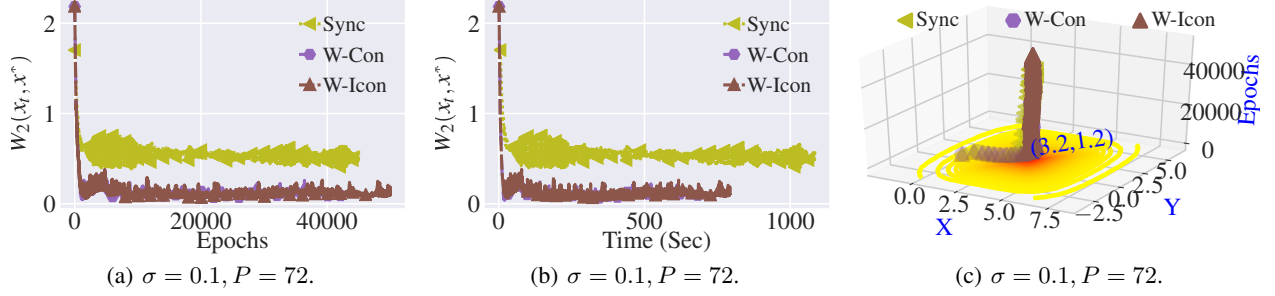


Figure 3: Optimization trajectory for training with 72 processes. Other descriptions are as those of Figure 1.

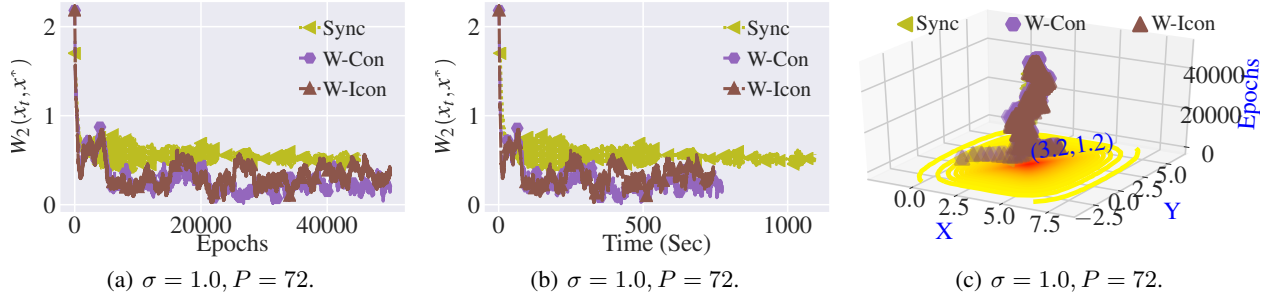


Figure 4: Optimization trajectory for 72 processes and $\nu_i \sim N(0, 1)$. Other descriptions are as those of Figure 1.

relative behavior of **Sync** in comparison to asynchronous methods is similar as before, however, with increased noise in the stochastic gradients, the read consistent method **W-Con** exhibits better convergence compared to **W-Icon**.

3.3 Reconstruction Independent Component Analysis (RICA)

For the second test case we considered reconstruction ICA [7]. The objective is defined as,

$$\min_W \lambda \|Wx\|_1 + \frac{1}{2} \|W^T Wx - x\|_2^2$$

where W are the features and x is the input vector. The first term penalizes for sparsity of the hidden representation Wx and the second is the Reconstruction ICA approach to relaxing the orthonormal constraint in regular ICA to a penalty term. We used $\lambda = 0.4$ in our experiments. The images from the well-known CIFAR10 dataset [6] are utilized for RICA. The experiments are implemented over the GPU-based shared-memory setting **M2**. We used an identical constant learning rate of 0.002 and a batch size of 1000 across the runs; the results are shown in Figures 5, 6, and 7 for $\nu_i \sim N(0, 0.01)$.

We observe that the relative experimental behavior of the methods over a GPU, where concurrency and resultant asynchrony thereof are too constrained, is different from that observed on setting **M1**. The asynchronous methods, though doing better in terms of speedup, under-perform the synchronous update scheme as we increase asynchrony from $P = 2$ to $P = 8$. It displays the impact of higher inconsistency due to delayed gradient updates. As CUDA runtime allows roughly identical parallelization to the concurrent processes, their speed-up performance are similar. To investigate the impact of noise in the updates, we conducted another set of experiments with $\nu_i \sim N(0, 0.0001)$, see Figure 8. Both the synchronous and asynchronous methods exhibit roughly identical convergence trajectory with respect to iterations, while the asynchronous ones obtain similar speed-up as before. Additional experimental results and descriptions thereof are available in Appendix B.

4 Conclusion

In this paper we analyzed the theoretical and numerical properties of SGLD with gradients computed at delayed iterates. We showed theoretically and numerically that the distributions of iterates approached the stationary distribution at a reasonable rate, i.e., of the same order of magnitude of iterations as the synchronous version, suggesting the potential of speedup in wall clock time.

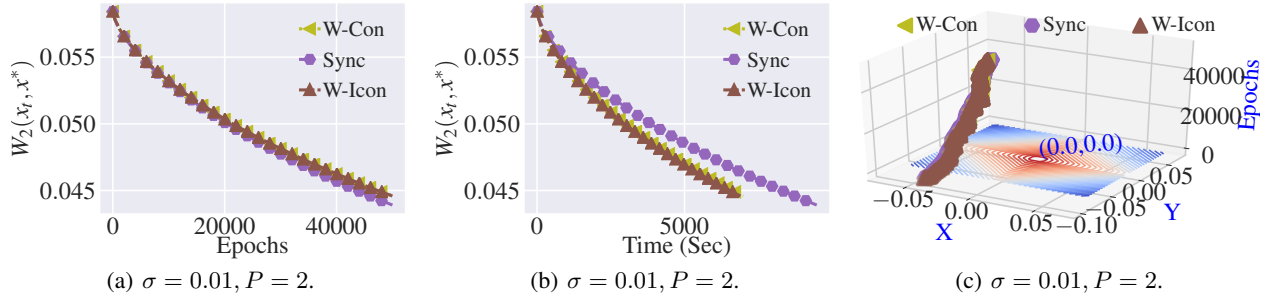


Figure 5: Optimization trajectory of the SGLD iterates for RICA are shown for training with 2 concurrent processes over a GPU. The description of sub-figures are as those of Figure 1.

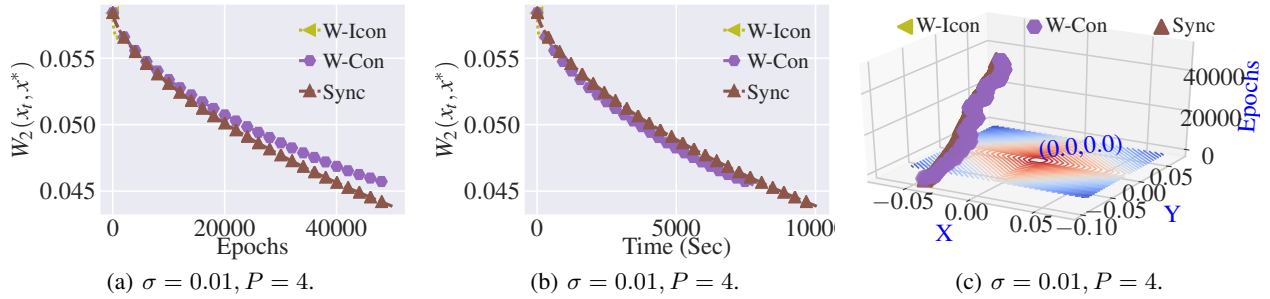


Figure 6: Trajectory of the distance of SGLD iterates from the optimal of SGLD.

References

- [1] Changyou Chen, Nan Ding, Chunyuan Li, Yizhe Zhang, and Lawrence Carin. Stochastic gradient mcmc with stale gradients. In *Advances in Neural Information Processing Systems*, pages 2937–2945, 2016.
- [2] Xiang Cheng, Niladri S Chatterji, Peter L Bartlett, and Michael I Jordan. Underdamped langevin mcmc: A non-asymptotic analysis. *arXiv preprint arXiv:1707.03663*, 2017.
- [3] Arnak S Dalalyan and Avetik Karagulyan. User-friendly guarantees for the langevin monte carlo with inaccurate gradient. *Stochastic Processes and their Applications*, 129(12):5278–5311, 2019.
- [4] Alain Durmus, Szymon Majewski, and Blazej Miasojedow. Analysis of langevin monte carlo via convex optimization. *Journal of Machine Learning Research*, 20(73):1–46, 2019.
- [5] R’emi Flamary and Nicolas Courty. Pot python optimal transport library, 2017.
- [6] Alex Krizhevsky and Geoffrey Hinton. Learning multiple layers of features from tiny images. 2009.
- [7] Quoc V. Le, Alexandre Karpenko, Jiquan Ngiam, and Andrew Y. Ng. ICA with reconstruction cost for efficient overcomplete feature learning. In *NIPS*, pages 1017–1025, 2011.
- [8] Chunyuan Li, Changyou Chen, Yunchen Pu, Ricardo Henao, and Lawrence Carin. Communication-efficient stochastic gradient mcmc for neural networks. In *Association for the Advancement of Artificial Intelligence*, 2019.
- [9] Adam Paszke, Sam Gross, Soumith Chintala, Gregory Chanan, Edward Yang, Zachary DeVito, Zeming Lin, Alban Desmaison, Luca Antiga, and Adam Lerer. Automatic differentiation in pytorch. 2017.
- [10] Maxim Raginsky, Alexander Rakhlin, and Matus Telgarsky. Non-convex learning via stochastic gradient langevin dynamics: a nonasymptotic analysis. *arXiv preprint arXiv:1702.03849*, 2017.
- [11] Herbert Robbins and Sutton Monro. A stochastic approximation method. *The annals of mathematical statistics*, pages 400–407, 1951.
- [12] Max Welling and Yee W Teh. Bayesian learning via stochastic gradient langevin dynamics. In *Proceedings of the 28th international conference on machine learning (ICML-11)*, pages 681–688, 2011.
- [13] D. Randall Wilson and Tony R. Martinez. The inefficiency of batch training for large training sets. In *IJCNN*, pages 113–117, 2000.

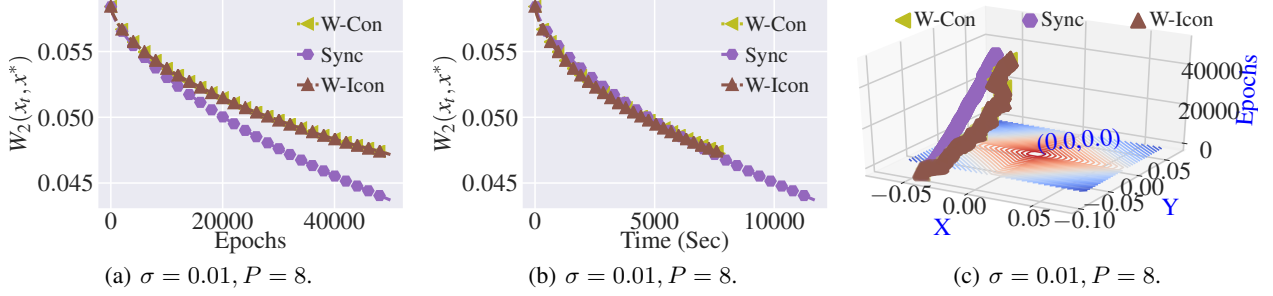
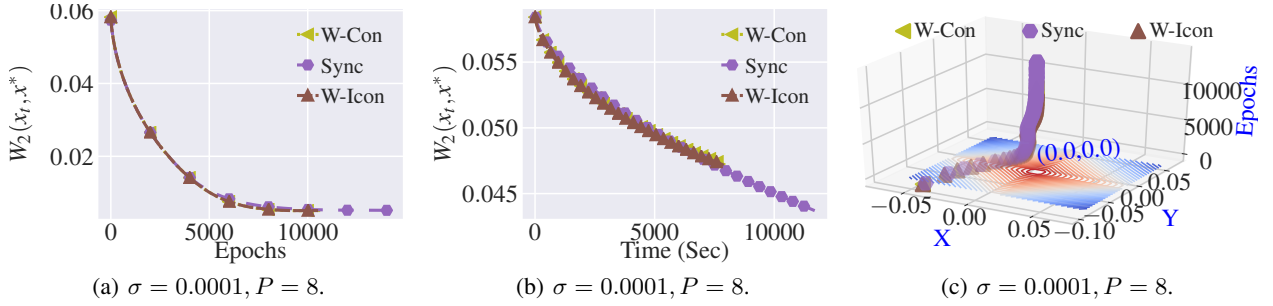


Figure 7: Trajectory of the distance of SGLD iterates from the optimal of SGLD.


 Figure 8: Optimization trajectory for 8 processes, $\nu_i \sim \mathcal{N}(0, 10^{-4})$. Other descriptions are as those of Figure 5.

A Convergence Proofs

A.1 Proof of Lemma 2.2

$$\begin{aligned}
 & U(x - \gamma \nabla U(\hat{x})) - U(y) = U(x - \gamma \nabla U(x)) - U(x - \gamma \nabla U(x)) + U(x - \gamma \nabla U(\hat{x})) - U(y) \\
 & \leq -\gamma(1 - \gamma L/2) \|\nabla U(x)\|^2 + \langle \nabla U(x), x - y \rangle - (m/2) \|y - x\|^2 \\
 & \quad + \gamma \langle \nabla U(x), \nabla U(x) - \nabla U(\hat{x}) \rangle + \gamma \langle \nabla U(x - \gamma \nabla U(x)) - \nabla U(x), \nabla U(x) - \nabla U(\hat{x}) \rangle \\
 & \quad + \frac{\gamma^2 L^2}{2} \|\nabla U(x) - \nabla U(\hat{x})\|^2 \\
 & \leq -\gamma(1 - \gamma L/2) \|\nabla U(x)\|^2 + \langle \nabla U(x), x - y \rangle - (m/2) \|y - x\|^2 + \frac{\gamma}{2} \|\nabla U(x)\|^2 \\
 & \quad + \frac{\gamma L^2}{2} \|x - \hat{x}\|^2 + \gamma^2 L^2 \|\nabla U(x)\| \|x - \hat{x}\| + \frac{\gamma^2 L^4}{2} \|x - \hat{x}\|^2
 \end{aligned}$$

Using Young's inequality on the second to last term and multiplying by 2γ we have,

$$\begin{aligned}
 & 2\gamma[U(x - \gamma \nabla U(\hat{x})) - U(y)] \\
 & \leq (1 - m\gamma) \|x - y\|^2 - \|x - \gamma \nabla U(x) - y\|^2 + \gamma^3(L + L^2) \|\nabla U(x)\|^2 \\
 & \quad + \gamma^2(L^2 + \gamma(L^2 + L^4)) \|x - \hat{x}\|^2 \\
 & \leq (1 - m\gamma) \|x - y\|^2 - (1 - \gamma) \|x - \gamma \nabla U(\hat{x}) - y\|^2 + \gamma^3(L + L^2) \|\nabla U(x)\|^2 \\
 & \quad + \gamma^2(L^2 + \gamma(L^2 + L^4)) \|x - \hat{x}\|^2 + \left(1 + \frac{1}{4\gamma}\right) \|\gamma \nabla U(x) - \gamma \nabla U(\hat{x})\|^2 \\
 & \leq (1 - m\gamma) \|x - y\|^2 - (1 - \gamma) \|x - \gamma \nabla U(\hat{x}) - y\|^2 + \gamma^3(L + L^2) \|\nabla U(x)\|^2 \\
 & \quad + \gamma \left(\frac{L^2}{4} + \gamma(2L^2 + \gamma(L^2 + L^4))\right) \|x - \hat{x}\|^2
 \end{aligned}$$

Let (X, Y) be an optimal coupling between μ and ν . Now take expectations with respect to μ and we have,

$$\begin{aligned}
 & 2\gamma[\mathbb{E}_{d\hat{\mu}}[\mathcal{E}(\mu \hat{S}_\gamma)] - \mathcal{E}(\nu)] \leq (1 - m\gamma) W_2^2(\mu, \nu) - (1 - \gamma) \mathbb{E} \|X - \gamma \nabla U(\hat{X}) - Y\|^2 \\
 & \quad + \gamma^3(L + L^2) \mathbb{E} \|\nabla U(X)\|^2 + \gamma \left(\frac{L^2}{4} + \gamma(2L^2 + \gamma(L^2 + L^4))\right) \mathbb{E} \|X - \hat{X}\|^2
 \end{aligned}$$

Using $W_2^2(\mu \hat{S}_\gamma, \nu) \leq \mathbb{E}_{d\mu} [\|X - \gamma \nabla U(\hat{X}) - Y\|^2]$ concludes the proof. \square

A.2 Proof of Theorem 2.1

Applying Lemma 1b in [4], the convexity of the KL divergence and Proposition 2.1 we get

$$\begin{aligned}
 KL(\nu_n^N | \pi) &\leq \Lambda_{N, N+n}^{-1} \sum_{k=N+1}^{N+n} \lambda_k KL(\mu_0 \hat{Q}_\gamma^k | \pi) \\
 &\leq (2\Lambda_{N, N+n})^{-1} \left[\frac{(1-m\gamma_{N+1})\lambda_{N+1}}{\gamma_{N+1}} W_2^2(\mu_0 \hat{Q}_\gamma^N, \pi) - \frac{\lambda_{N+n}}{\gamma_{N+n}} W_2^2(\mu_0 \hat{Q}_\gamma^{N+n}, \pi) \right. \\
 &\quad + \sum_{k=N+1}^{N+n-1} \left\{ \frac{(1-m\gamma_{k+1})\lambda_{k+1}}{\gamma_{k+1}} - \frac{\lambda_k}{\gamma_k} \right\} W_2^2(\mu_0 \hat{Q}_\gamma^k, \pi) + \sum_{k=N+1}^{N+n} Ld\lambda_k \gamma_k \\
 &\quad + \sum_{k=N+1}^{N+n} \lambda_k \gamma_k W_2^2(\mu_0 \hat{S}_\gamma^k, \pi) + \frac{1}{2} \sum_{k=N+1}^{N+n} \lambda_k \gamma_k^2 (L + L^2) \int_{\mathbb{R}^d} \|\nabla U(x)\|^2 d\mu_k(x) \\
 &\quad \left. + \frac{1}{2} \sum_{k=N+1}^{N+n} \lambda_k \left(\frac{L^2}{4} + 2\gamma_k L^2 + \gamma_k^2 (L^2 + L^4) \right) \int_{\mathbb{R}^d} \|x - \hat{x}\|^2 d\mu_k(x) \right]
 \end{aligned}$$

Now, with τ the maximum delay, we can write,

$$\begin{aligned}
 \mathbb{E} [\|x_k - \hat{x}_k\|^2] &\leq \sum_{l=k-\tau}^k \gamma_l \tau \mathbb{E} \left[\left\| \gamma_l^{1/2} \nabla U(\hat{x}_k) + \sqrt{2} G_{k+1} \right\|^2 \right] \\
 &\leq \sum_{l=k-\tau}^k \left[2\gamma_l^2 \tau \max_{s \in \{l-\tau, \dots, l\}} \mathbb{E} \|\nabla U(x_s)\|^2 + 4\gamma_l \tau \sigma \right] \\
 &\leq \sum_{l=k-\tau}^k \left[2\gamma_l^2 \tau \sum_{s=l-\tau}^l \mathbb{E} \|\nabla U(x_s)\|^2 \right] + 4\gamma_{k-\tau} \tau^2 \sigma
 \end{aligned}$$

and thus,

$$\begin{aligned}
 &\sum_{k=N+1}^{N+n} \lambda_k \left(\frac{L^2}{4} + 2\gamma_k L^2 + \gamma_k^2 (L^2 + L^4) \right) \int_{\mathbb{R}^d} \|x - \hat{x}\|^2 d\mu_k(x) \\
 &\leq \sum_{k=N+1-\tau}^{N+n} 2\lambda_k \gamma_k \tau^2 \left(\frac{L^2}{4} + 2\gamma_k L^2 + \gamma_k^2 (L^2 + L^4) \right) \left[\gamma_k \int_{\mathbb{R}^d} \|\nabla U(x)\|^2 d\mu_k(x) + 2\sigma \right]
 \end{aligned}$$

from which the final result follows. \square

A.3 Proof of Corollary 2.1

Assumption 2.2 and following the proof of Theorem 2.1 while setting $\lambda_k = 1$ gives,

$$\begin{aligned}
 nKL(\nu_n^N | \pi) + W_2^2(\mu_0 \hat{Q}_\gamma^{N+n}, \pi) / (2\gamma) &\leq (1-m\gamma) W_2^2(\mu_0 Q_\gamma^N, \pi) / (2\gamma) \\
 + Ldn\gamma + 2 \left(\frac{L^2}{4} + 2\gamma L^2 + \gamma^2 (L^2 + L^4) \right) \tau^2 \sigma (n + \tau) \gamma \\
 + \gamma^2 \left[\frac{L}{2} + \frac{L^2}{2} + \tau^2 \left(\frac{L^2}{4} + 2\gamma L^2 + \gamma^2 (L^2 + L^4) \right) \right] G^2(n + \tau) + \gamma \sum_{k=N+1}^{N+n} W_2^2(\mu_0 \hat{S}_\gamma^k, \pi)
 \end{aligned}$$

Now we use [3] to derive a bound on the last term, considering the constant step-size stochastic gradient Langevin with delayed gradients as an innacurate biased gradient version of Langevin dynamics, as considered in that paper, and defining the convergence in Wasserstein norm.

In particular, using Theorem 4 in [3] with the gradient inaccuracy bias,

$$\|\nabla U(X_k) - \nabla U(\hat{X}_k)\| \leq L\tau(\gamma G + \sqrt{\gamma\sigma})$$

and variance as simply 2σ , we get that,

$$\gamma \sum_{k=N+1}^{N+n} W_2^2(\mu_0 \hat{S}_\gamma^k, \pi) \leq \frac{\mathbb{E}[W_2^2(\mu_0)]}{1-m\gamma} + 1.65(L/m)\gamma^{3/2}n + \frac{\gamma L\tau(\gamma G + \sqrt{\sigma\gamma})n}{m} + \frac{2\gamma^{3/2}\sigma n}{1.65L + \sqrt{\sigma\gamma m}}$$

The rest of the proof follows from setting $N = 1$, the choice of γ_ϵ and the fact that both the KL divergence and Wasserstein norms are positive. \square

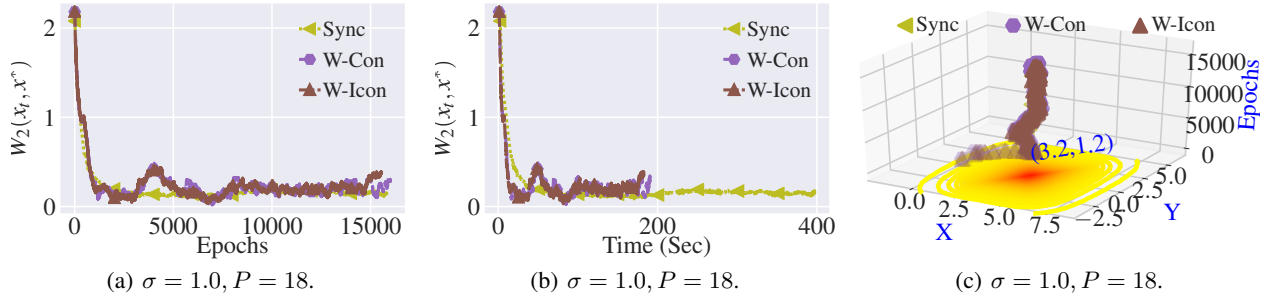


Figure 9: Optimization trajectory of the SGLD iterates for regression experiment are shown for training with 18 processes on CPU and $\nu_i \sim N(0, 1)$. Sub-figure (a) shows the convergence with respect to iterations (epochs), whereas, sub-figure (b) presents relative speed-up of the methods. In sub-figure (c), we depict the trajectory of iterates by tracking their first two co-ordinates. Sub-figure (c) also presents the contour plot of the potential $\exp(-U(x))$ near x^* on the plane $Epoch = 0$.

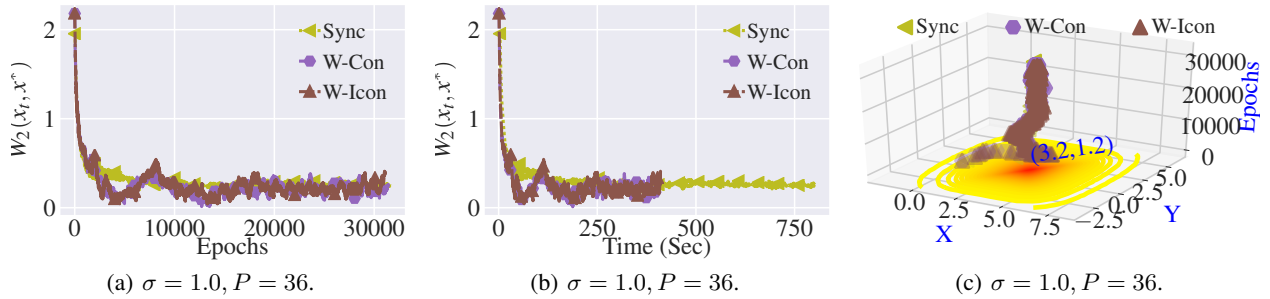


Figure 10: Optimization trajectory of the SGLD iterates for regression experiment with 36 processes on CPU and $\nu_i \sim N(0, 1)$. Other descriptions are the same as those of Figure 9.

B Additional Numerical Experiments

In this section we present some additional numerical results. Firstly, the remaining results from Section 3.3. see Figures 9, 10, 11 and 12. Essentially, we observe that for a higher noise, in Figures 9 and 10, the convergence behavior of synchronous and asynchronous methods become more similar for relatively lower asynchrony: compare it against Figure 4 in Section 3 in the paper. On the other hand, we observe that in comparison to the CPU-based asynchrony, the GPU-based asynchrony does not cause different behavior in terms of per epoch convergence for the asynchronous and synchronous methods as the noise is reduced. However, in terms of speed-up, the asynchronous methods are still faster compared to the synchronous method, see 11 and 12.

Further, we present the numerical results with respect to norm distance between iterates and the posterior. The experiments of regression are presented in Figures 13 to 17.

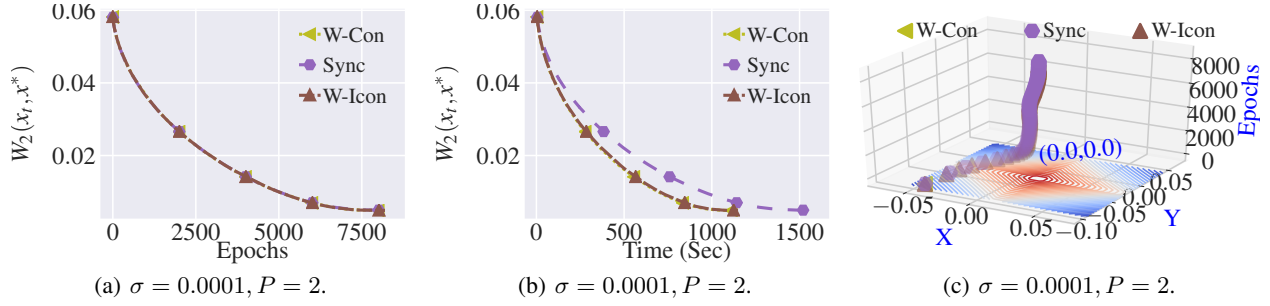


Figure 11: Optimization trajectory of the SGLD iterates for RICA experiment with 2 concurrent processes on GPU and $\nu_i \sim N(0, 0.0001)$. Other descriptions are the same as those of Figure 9.

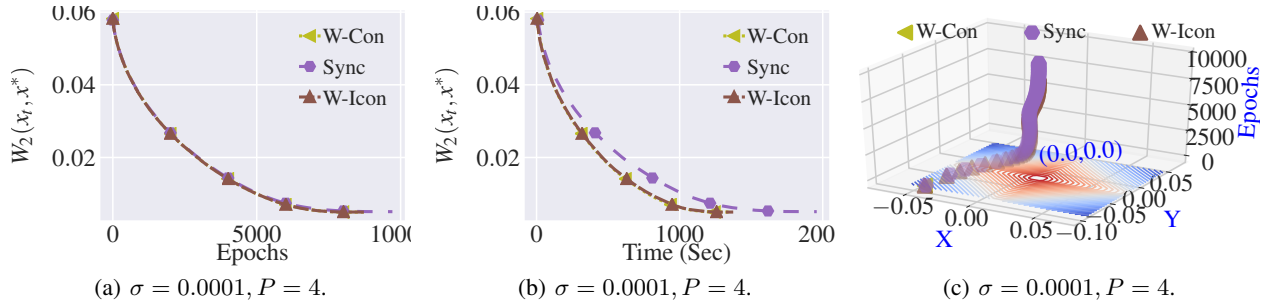


Figure 12: Optimization trajectory of the SGLD iterates for RICA experiment with 4 concurrent processes on GPU and $\nu_i \sim N(0, 0.0001)$. Other descriptions are the same as those of Figure 9.

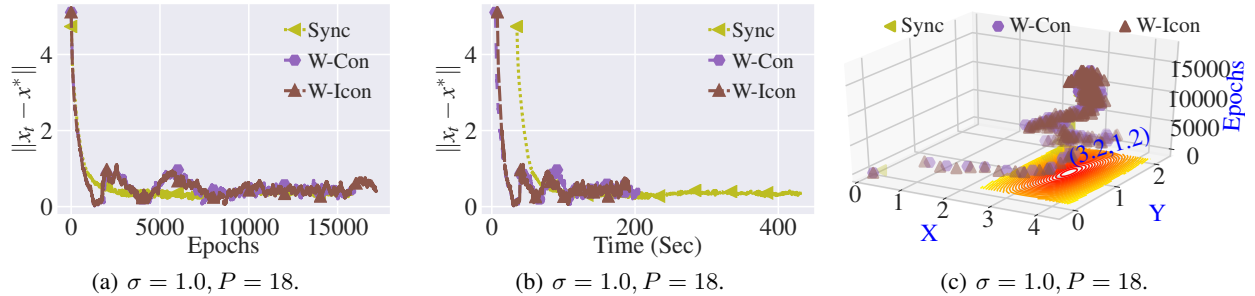


Figure 13: Optimization trajectory of the SGLD iterates for regression experiment with 18 processes on CPU and $\nu_i \sim N(0, 1)$. Other descriptions are the same as those of Figure 9.

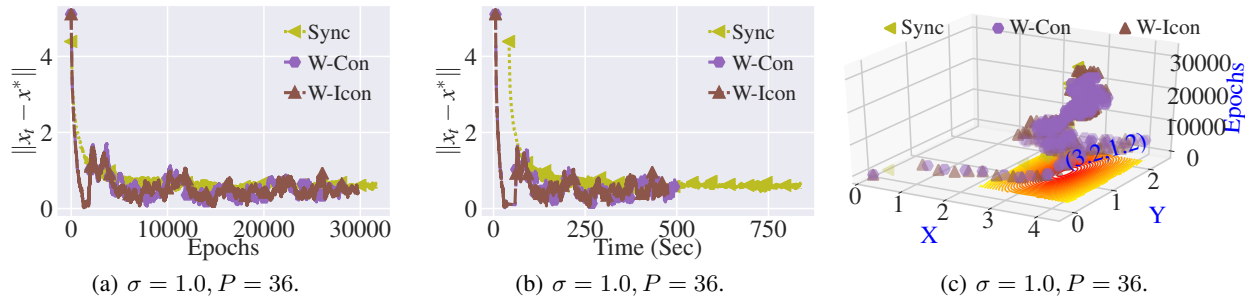


Figure 14: Optimization trajectory of the SGLD iterates for regression experiment with 36 processes on CPU and $\nu_i \sim N(0, 1)$. Other descriptions are the same as those of Figure 9.

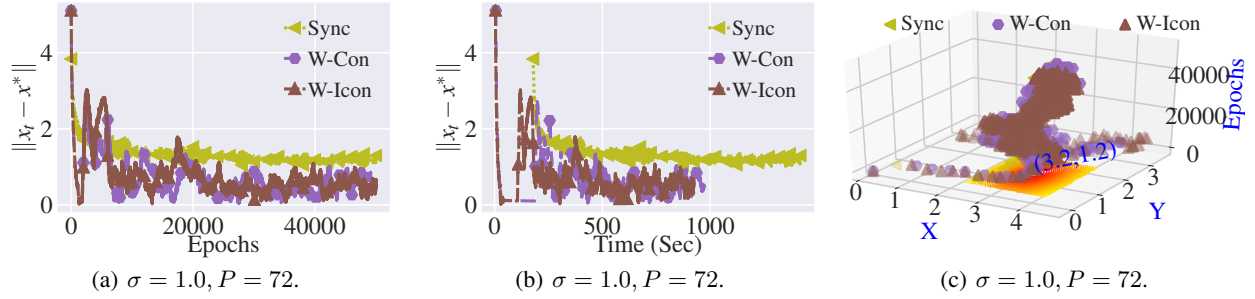


Figure 15: Optimization trajectory of the SGLD iterates for regression experiment with 72 processes on CPU and $\nu_i \sim N(0, 1)$. Other descriptions are the same as those of Figure 9. Notice that with higher asynchrony the convergence of large batch synchronous method gets poorer.

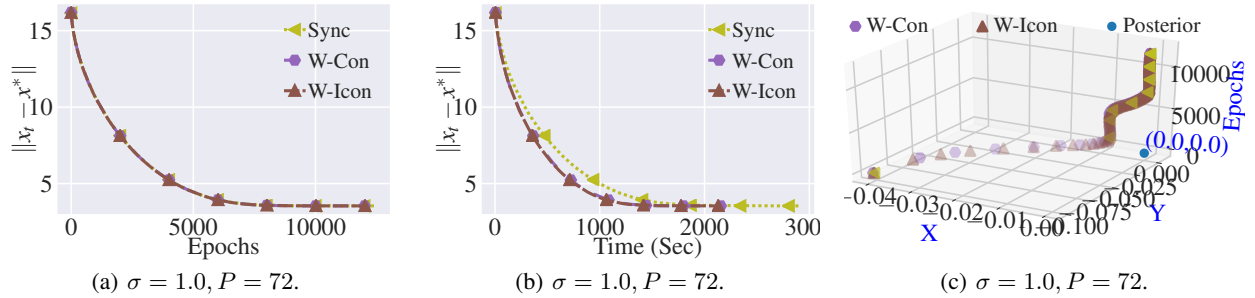


Figure 16: Optimization trajectory of the SGLD iterates for RICA experiment with 2 processes on GPU and $\nu_i \sim N(0, 0.01)$. Other descriptions are the same as those of Figure 9.

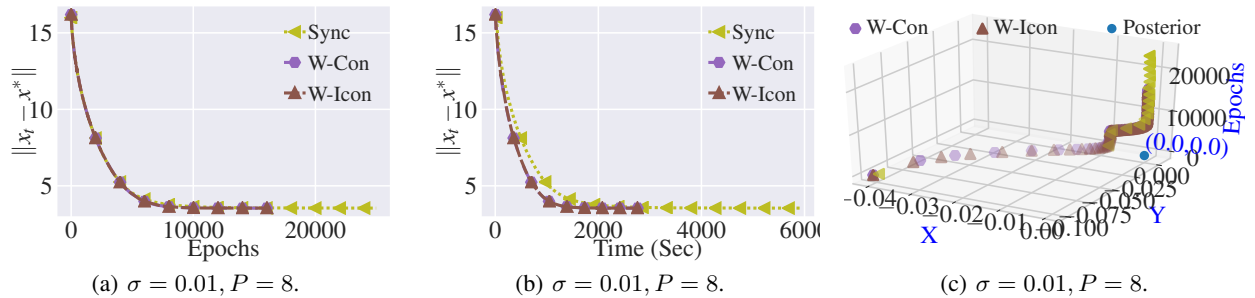


Figure 17: Optimization trajectory of the SGLD iterates for RICA experiment with 8 processes on GPU and $\nu_i \sim N(0, 0.01)$. Other descriptions are the same as those of Figure 9.